Refractive Index Sensor by Interrogation of Etched MgO Nanoparticle-Doped Optical Fiber Signature

Sanzhar Korganbayev, Madina Shaimerdenova, Takhmina Ayupova, Marzhan Sypabekova, Aliya Bekmurzayeva, Wilfried Blanc, Carlo Molardi, and Daniele Tosi

***Abstract*— Traditional fiber-optic refractive index (RI) sensors require a reflective or resonant device in fiber (such as a grating, an interferometer, a taper, or a plasmonic device) and a spectral domain detection. In this letter, we demonstrate and experimentally validate, the possibility to fabricate a minimalistic RI sensor, based on the wet-etching of an enhanced backscattering fiber made with a core doped with MgO-based-nanoparticles. Interrogation is performed in the length domain, by detecting and correlating the random losses of the fiber with an optical backscatter reflectometer. The sensitivity is 5.25 mm/RIU with 9.6 μm resolution, corresponding to 9.69 ps/RIU.**

***Index Terms*— Refractive index sensor, optical fiber sensor, distributed sensing, specialty fibers.**

I. Introduction

FIBER optic refractive index (RI) sensors are an important technology for modern detection, as they allow environmental sensing of the RI of liquid [1] and gases [2] with a compact probe, and with high sensitivity. Most notably, RI sensors constitute the building block of fiber optic biosensors, which in most cases are RI sensors biologically functionalized for the selective detection of analytes through functional bioreceptors [3].

RI sensors and biosensors typically operate under two conditions: (1) they require an in-fiber device that acts as a reflection or transmission filter, altering the spectrum of the reflected or transmitted light; (2) they perform a detection in the optical spectrum domain, with instruments such as optical spectrum analyzer (OSA) [4], optical vector analyzer (OVA) [5], or an optoelectronic interrogator [6].

The fabrication of RI sensors and biosensors is therefore dependent upon the in-fiber device. The majority of RI sensors can be divided into two groups. The first class of sensors use fiber gratings, which are fabricated by direct inscription through phase mask or with a fs laser [7]; in this framework, RI sensors based on tilted fiber Bragg grating (TFBG) [8], etched fiber Bragg grating (EFBG) [9], and long-period grating (LPG) [6] have been reported. The second group of RI sensors is based on micro-structures, exhibiting a resonant or periodic behavior; in this group of sensors we can find surface plasmon resonance (SPR) [10], fiber tapers [11], single-multi-single mode (SMS) interferometers [12]. Inline interferometers are fabricated using fusion or CO_2 laser splicers, while plasmonic devices require the deposition of thin metallic films with sub-wavelength thickness.

The spectral interrogation of the RI sensors represents the golden standard for detection; a common feature of sensors is that the sensitivity is expressed in nm/RIU (refractive index units) and represents the relative wavelength shift of the spectra of the sensing devices [1]–[12]. This method of detection is reliable and robust, as it does not depend on the power stability of the optical source which cannot be guaranteed over long term.

A major drawback for the development of a low-cost yet reliable fiber-optic biosensor is the requirement to fabricate a device in the fiber. This operation is often not easy and not scalable, as the fabrication of each reflector requires precision micromachining. To cope with this drawback, a first attempt to simplify the structure of a RI sensor has been performed by Sypabekova *et al.* [13], who reported a spectrally operated RI sensor based on the interrogation of Rayleigh scattering signature in a wet-etched fiber. As opposite to gratings, interferometers, and plasmonic devices, wet-etching is a scalable process often used in mass production of electronic circuits [14], etching of photoresists [15], and metal oxide removal [16].

In this Letter, we introduce a novel method for developing a minimalistic RI sensor, with a one-step wet-etching fabrication and a referenced detection. The architecture is "reflector-less", as effectively we are not inscribing a reflective element in the fiber but rather using the Rayleigh scattering as processed information. The demodulation is performed in the time domain, measuring the scattering power traces of an enhanced backscattering fiber (EBF): the delay due to the effective refractive index change shifts the scattering traces of

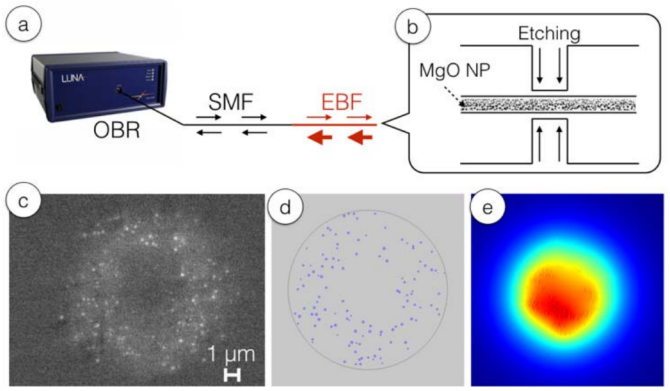

Fig. 1. Schematic and working principle of the refractive index sensor and the EBF fiber. (a) Schematic of the OBR setup; (b) schematic of the etched MgO-NP etched fiber sensor; (c) SEM view of the MgO-NP fiber; (d) core cross-section of a MgO-NP fiber with the same NP size and distribution; (e) simulated LP_{01}-like mode.

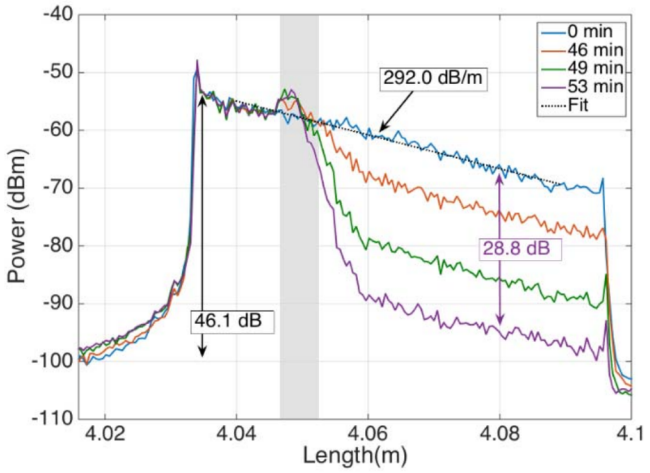

Fig. 2. Backscattering traces during etching, reporting the received backscattered power as a function of length before etching (0 min), during etching (46 min, 49 min) and at the end of the etching process (53 min). The shadow area represents the etched region.

the fiber, and we can detect it using an optical backscatter reflectometer (OBR).

II. Experimental Setup and Results

The setup of the system is sketched in Fig. 1(a). The analyzer is an OBR (Luna OBR4600, Luna Inc., US) which is based on a coherent optical frequency domain reflectometer (OFDR) [17]–[18]. The following parameters have been used in experiments: scan range 1525.0 – 1610.5 nm, effective refractive index 1.454, sensing length 6.5 cm, 10130 sensing points. The EBF fiber [19] used for sensing is a MgO-nanoparticle-doped fiber (MgO-NP) [20], having enhanced light backscattering with respect to a standard single mode fiber (SMF). The EBF, presenting the same core and cladding size of an SMF-28, has been easily spliced to a lead-out SMF fiber, using a standard fusion splicer (Fujikura 12-S, SMF-SMF splice recipe).

The fiber has been functionalized to refractive index sensing by means of wet etching, in hydrofluoric acid (HF) [6], [13]. The etched fiber was 1 cm in length (1.5 cm away from spliced region), resulting in an increase of evanescent waves in correspondence to the etched location. Etching has been performed in a fume hood (Waldner Secuflow airflow controller), using 48% and 24% HF (Sigma-Aldrich, at room temperature) for 30 and for 23 minutes respectively.

The nanoparticle properties are mainly dependent on the Mg concentration. By tailoring the doping of the preform it is possible to vary particle size and density. Fig. 1(c) shows the scanning electron microscopy (SEM) view of the fiber section. A fiber with a profile having a similar random distribution of nanoparticles (same concentration and same size statistics) has been simulated by the use of a Finite Element Method (FEM) based software. The cross-section of the simulated fiber with NP forming a ring-shaped structure around the inner part of the core is shown in Fig. 1(d). For the simulation an increase of refractive index of 3×10^{-3} has been chosen for the RI difference between the core and the cladding, while the nanoparticle refractive index is a random value between 1.53 to 1.65. Simulations have been performed at an operation wavelength of 1550 nm. As a result, Fig. 1(e) shows the fundamental LP_{01}-like mode of the fiber. The presence of NP induces a deformation of the mode shape. A significant increase of the mode confinement, that can be explained with the localization effect [21], is also detected. The integral overlap of the normalized intensity over the core, as defined in [22], assumes a value of 0.83. As a comparison, a SMF fiber with the same core diameter, but without nanoparticle doping, presents a core overlap of 0.71.

The results of the sensor fabrication are reported in Fig. 2, which shows the backscattering traces, i.e. received power as a function of fiber length in the fiber; for better visualization the resolution has been increased to 0.49 mm. The EBF is connected at the length of 4.034 m, which results in a steep increase of the backscattered power. We estimate the backscattering gain, i.e. the difference between the SMF scattering power (−99.0 dBm) and the EBF scattering power (−52.9 dBm) to 46.1 dB. Conversely, the linear fit shows a high loss in the EBF, estimated as 292.0 dB/m accounting for both forward and backward signals. The sensor is etched for a length of 1 cm in correspondence of the length 4.048 m. As etching progresses, the trace is altered from the initial shape, showing a slight increase of backscattered power in the etched part (as in [13], this is due to a slight change of backscattered power in the lead-in etched section), followed by a decrease of power due to the increase of evanescent signal. The sensor appears to be sensitive after approximately 40 min of etching. After 43 min elapsed in HF etchant, the difference in received power (estimated at the length of 4.08 m) is 7.8 dB, and it increases to 19.5 dB after 46 min. We stop the etching process after 53 min, with a loss differential of 28.8 dB. The whole etching process has been monitored in real time through the OBR, using the differential loss shown in Fig. 2 as the key metric.

We remark that it is necessary to employ an EBF fiber for this setup, as the additional losses introduced by fiber etching are large and would not be sustainable by a SMF fiber since the limit of the detection of the OBR is ≈ -110 dBm. On the other hand, the MgO-doped EBF has a large scattering increment

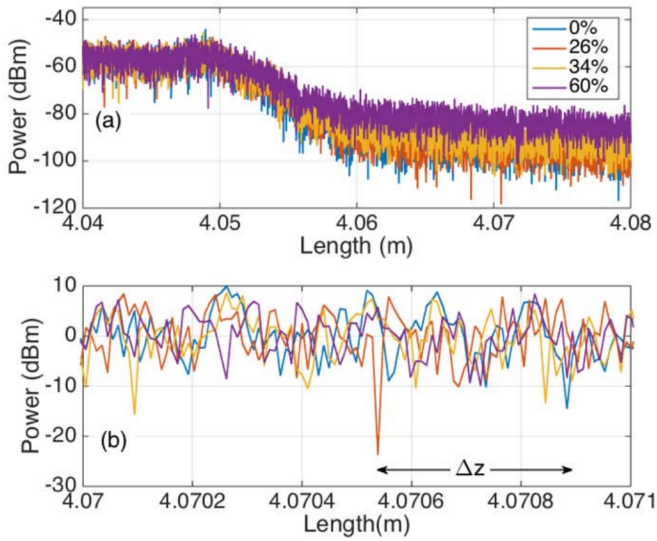

Fig. 3. Dependence of the backscattering traces on the refractive index. (a) Backscattering traces observed in correspondence of the etched region and afterwards, for different concentrations of sucrose/water (0%, 26%, 34%, 60%) corresponding to refractive indexes 1.3330, 1.3741, 1.3885, 1.4419; (b) backscattering traces after high-pass filtering, zoomed in a short region where we can observe the spatial differential Δz.

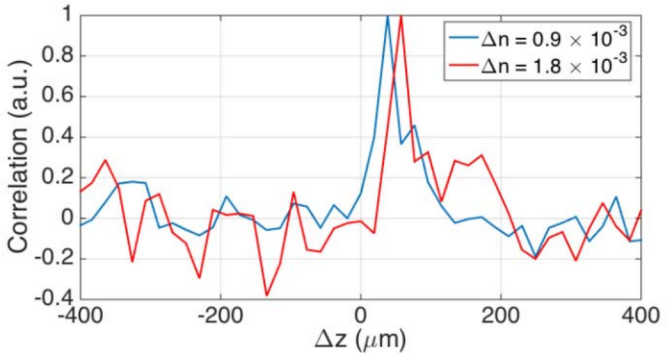

Fig. 4. Correlation between the reference trace and the measured trace, after high-pass filtering, for two values of RI change Δn.

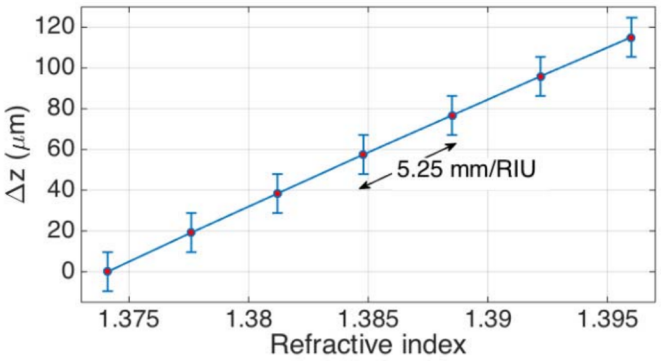

Fig. 5. Evaluation of the spatial change Δz as a function of the refractive index, varying the solutions of sucrose from 26% to 38%.

that raises the power detected by the OBR, compensating for both the fiber losses and the evanescent field in the etched region.

Fig. 3(a) shows how the traces (backscattered power as a function of length) change as a function of the refractive index, which varies $\approx 1.85 \times 10^{-3}$ for each 1% of sucrose. At first, we observe that after the etched region, the backscatter level has a different value, due to the difference in evanescent power [6]. However, we can also observe that the change of effective RI in the etched region due to the change of surrounding RI results in a time delay which depends on the RI itself. Due to the fluctuations of local losses, which is caused by random changes of nanoparticle size, distribution, and location the backscattered signal appears as a fluctuating signal, which shifts as a function of the RI. This is the key of the interrogation method proposed in this Letter: while in [13] and [17] the signature is detected in the frequency domain, measuring the wavelength shift of each signature, in this work we operate in the time domain, detecting the time (or length) delay introduced by the etched fiber directly in the backscattering trace. Prior to analyze the traces, we perform a digital high-pass filtering (Butterworth finite impulse response, 5^{th} order, high-pass normalized frequency 0.005) in order to remove the dependence on the power level and have better referencing of the signals. The resulting traces are shown in Fig. 3(b), where we show that, for each RI, we observe a different spatial delay Δz.

The signal in Fig, 3(b) is therefore treated as a "loss signature" of the fiber and is recorded in the region following the etched part. In the etched region, the change of effective refractive index provides a variable delay to the loss signature.

In order to estimate Δz, we can estimate the mutual correlation between the reference trace (acquired at the reference RI value), and the measured trace. We obtain a signal with a distinct peak in correspondence of the estimated value of Δz; this technique, in the time domain, is the correspondence of the estimation of the wavelength shift by correlating spectral traces [17]. The result, for two variations of RI difference (Δn), is reported in Fig. 4: as the RI changes, the correlation peak shifts towards the longer lengths due to the incremental delay in the light propagation through the etched region.

In order to reproduce the typical working condition of a refractive index sensor, we show in Fig, 5 the variation of Δz as a function of the RI change for relatively small changes of RI. In this experiment, the sensor has been introduced in liquids having RI changing from 1.3741 (26% sucrose) to 1.3960 (38% sucrose) in steps of 2%. We observe that the relationship between the differential length Δz and the RI is linear, with an estimated sensitivity $\Delta z/\Delta n$ equal to 5.25 mm/RIU. The resolution of the method is dependent on the minimum spacing that the OBR can detect. According to [18], the resolution of the OBR and any coherent OFDR is equal to $\Delta z_{min} = c/(2 \cdot n_{eff} \cdot \Delta f)$, where c is the speed of light, n_{eff} is the effective refractive index of the fiber, and Δf is the frequency range of the swept source. In the proposed setup, $n_{eff} = 1.454$ and $\Delta f = 10.67$ THz (equivalent to 85.5 nm centered at 1550 nm), thus $\Delta z_{min} = 9.6 \mu$m. The error bars in Fig. 5 reproduce the resolution of the method.

The proposed method shifts the sensitivity from the spectral domain, measured in nm/RIU (i.e. nm of wavelength shift of spectral dips or peaks per each RI change), which is

used in RI sensors and biosensors [1]–[12] as a benchmark, to a sensitivity in mm/RIU (i.e. mm of differential length Δz per one RIU variation). This is equivalent to express the sensitivity in time units: operating the conversion for the previous n_{eff} value, the sensitivity is 9.69 ps/RIU. In our work, we programmed the OBR to detect using the mm/RIU figure since the instrument operates directly on the scattering traces; the expression of the sensitivity in ps/RIU is however formally more correct, because it removes the dependence on the fiber n_{eff} value.

We estimate the thermal detuning error, introduced by effect of the thermal dependence of the effective refractive index and of the thermal expansion of the fiber, as $\approx 9.8 \times 10^{-2}$ RIU/°C

We remark that the key improvement of the method presented in this Letter with respect to [13] is that we can introduce an even more minimalistic sensing feature, that not only negates the need of inscribing a reflective or plasmonic device in the fiber, but also removes the need of spectral detection. This method is potentially compatible with microwave photonics detection systems, which are simpler and more inexpensive than standard OBR interrogators.

III. Conclusion

In conclusion, this Letter demonstrates a fiber-optic RI sensor that does not require neither the fabrication of a reflective element, nor the detection of optical spectrum. The RI sensitivity is introduced by simply wet-etching a small portion of the fiber, without inscribing any device. The fiber used in experiments is a high-scattering fiber doped with MgO nanoparticles in the core, which allows having a backscatter signal capable of sustaining the evanescent field losses. Interrogation is performed in the time-domain, detecting the correlation between the backscattering signatures in the optical length domain. The estimated sensitivity is 5.25 mm/RIU. Overall, the proposed method is a minimalistic RI sensor: it is scalable for volume manufacturing like HF etching methods, and at the same time it simplifies the OBR hardware by negating the need for spectral detection.

References

[1] M. S. A. Gandhi, S. Chu, K. Senthilnathan, P. R. Babu, K. Nakkeeran, and Q. Li, "Recent advances in plasmonic sensor-based fiber optic probes for biological applications," *Appl. Sci.*, vol. 9, no. 5, p. 949, 2019.

[2] D.-W. Duan, Y.-J. Rao, L.-C. Xu, T. Zhu, D. Wu, and J. Yao, "In-fiber Mach-Zehnder interferometer formed by large lateral offset fusion splicing for gases refractive index measurement with high sensitivity," *Sens. Actuators B, Chem.*, vol. 160, no. 1, pp. 1198–1202, 2011.

[3] A. Leung, P. M. Shankar, and R. Mutharasan, "A review of fiber-optic biosensors," *Sens. Actuators B, Chem.*, vol. 125, no. 2, pp. 688–703, 2007.

[4] D. Sun, T. Guo, Y. Ran, Y. Huang, and B.-O. Guan, "*In-situ* DNA hybridization detection with a reflective microfiber grating biosensor," *Biosensors Bioelectron.*, vol. 61, pp. 541–546, Nov. 2014.

[5] C. Caucheteur, Y. Shevchenko, L.-Y. Shao, M. Wuilpart, and J. Albert, "High resolution interrogation of tilted fiber grating SPR sensors from polarization properties measurement," *Opt. Express*, vol. 19, no. 2, pp. 1656–1664, 2011.

[6] F. Esposito, L. Sansone, C. Taddei, S. Campopiano, M. Giordano, and A. Iadicicco, "Ultrasensitive biosensor based on long period grating coated with polycarbonate-graphene oxide multilayer," *Sens. Actuators B, Chem.*, vol. 274, pp. 517–526, Nov. 2018.

[7] X. Fang, C. R. Liao, and D. N. Wang, "Femtosecond laser fabricated fiber Bragg grating in microfiber for refractive index sensing," *Opt. Lett.*, vol. 35, no. 7, pp. 1007–1009, Apr. 2010.

[8] C. Ribaut *et al.*, "Cancer biomarker sensing using packaged plasmonic optical fiber gratings: Towards *in vivo* diagnosis," *Biosensors Bioelectron.*, vol. 92, pp. 449–456, Jun. 2017.

[9] A. Bekmurzayeva *et al.*, "Etched fiber Bragg grating biosensor functionalized with aptamers for detection of thrombin," *Sensors*, vol. 18, no. 12, p. 4298, 2019.

[10] B. D. Gupta and R. Kant, "Recent advances in surface plasmon resonance based fiber optic chemical and biosensors utilizing bulk and nanostructures," *Opt. Laser Technol.*, vol. 101, pp. 144–161, May 2018.

[11] Y. Huang *et al.*, "High-sensitivity DNA biosensor based on optical fiber taper interferometer coated with conjugated polymer tentacle," *Opt. Exp.*, vol. 23, no. 21, pp. 26962–26968, Oct. 2015.

[12] M. Olivero, A. Vallan, R. Orta, and G. Perrone, "Single-mode-multimode-single-mode optical fiber sensing structure with quasi-two-mode fibers," *IEEE Trans. Instrum. Meas.*, vol. 67, no. 5, pp. 1223–1229, May 2018.

[13] M. Sypabekova *et al.*, "Fiber optic refractive index sensors through spectral detection of Rayleigh backscattering in a chemically etched MgO-based nanoparticle-doped fiber," *Opt. Lett.*, vol. 43, no. 24, pp. 5945–5948, 2018.

[14] M. Datta and L. T. Romankiw, "Application of chemical and electrochemical micromachining in the electronics industry," *J. Electrochem. Soc.*, vol. 136, no. 6, pp. 285C–292C, 1989.

[15] G. A. C. M. Spierings, "Wet chemical etching of silicate glasses in hydrofluoric acid based solutions," *J. Mater. Sci.*, vol. 28, no. 23, pp. 6261–6273, 1993.

[16] K. R. Williams, K. Gupta, and M. Wasilik, "Etch rates for micromachining processing-Part II," *J. Microelectromech. Syst.*, vol. 12, no. 6, pp. 761–778, Dec. 2003.

[17] M. Froggatt, "Distributed measurement of the complex modulation of a photoinduced Bragg grating in an optical fiber," *Appl. Opt.*, vol. 35, no. 25, pp. 5162–5164, Sep. 1996.

[18] X. Bao and L. Chen, "Recent progress in distributed fiber optic sensors," *Sensors*, vol. 12, no. 7, pp. 8601–8639, Jun. 2012.

[19] A. Yan *et al.*, "Distributed optical fiber sensors with ultrafast laser enhanced Rayleigh backscattering profiles for real-time monitoring of solid oxide fuel cell operations," *Sci. Rep.*, vol. 7, no. 1, p. 9360, 2017.

[20] W. Blanc *et al.*, "Fabrication of rare earth-doped transparent glass ceramic optical fibers by modified chemical vapor deposition," *J. Amer. Ceram. Soc.*, vol. 94, no. 8, pp. 2315–2318, 2011.

[21] B. Abaie, E. Mobini, S. Karbasi, T. Hawkins, J. Ballato, and A. Mafi, "Random lasing in an Anderson localizing optical fiber," *Light Sci. Appl.*, vol. 6, Aug. 2017, Art. no. e17041.

[22] C. Molardi, F. Poli, L. Rosa, S. Selleri, and A. Cucinotta, "Mode discrimination criterion for effective differential amplification in Yb-doped fiber design for high power operation," *Opt. Express*, vol. 25, no. 23, pp. 29013–29025, 2017.